



This is a repository copy of *A transferable force-field for alkali metal nitrates*.

White Rose Research Online URL for this paper:
<https://eprints.whiterose.ac.uk/187218/>

Version: Published Version

Article:

Fantauzzo, V., Yeandel, S.R. orcid.org/0000-0002-6977-1677, Freeman, C.L. orcid.org/0000-0002-6326-1211 et al. (1 more author) (2022) A transferable force-field for alkali metal nitrates. *Journal of Physics Communications*, 6 (5). 055011. ISSN 2399-6528

<https://doi.org/10.1088/2399-6528/ac6e2b>

Reuse

This article is distributed under the terms of the Creative Commons Attribution (CC BY) licence. This licence allows you to distribute, remix, tweak, and build upon the work, even commercially, as long as you credit the authors for the original work. More information and the full terms of the licence here:
<https://creativecommons.org/licenses/>

Takedown

If you consider content in White Rose Research Online to be in breach of UK law, please notify us by emailing eprints@whiterose.ac.uk including the URL of the record and the reason for the withdrawal request.



eprints@whiterose.ac.uk
<https://eprints.whiterose.ac.uk/>

PAPER • OPEN ACCESS

A transferable force-field for alkali metal nitrates

To cite this article: V Fantauzzo *et al* 2022 *J. Phys. Commun.* **6** 055011

View the [article online](#) for updates and enhancements.

You may also like

- [Improvement of Oxygen Surface Exchange Kinetics for CGO with Surface Treatment](#)
J. Druce and J. A. Kilner
- [Design and Fabrication of a Highly Stable Polymer Carbon Nanotube Nanocomposite Chemiresistive Sensor for Nitrate Ion Detection in Water](#)
Ashwini N. Mallya and Praveen C. Ramamurthy
- [Local formation of sulfates contributes to the urban haze with regional transport origin](#)
Yong Bin Lim, Jihoon Seo, Jin Young Kim et al.



PAPER

A transferable force-field for alkali metal nitrates

OPEN ACCESS

RECEIVED
14 February 2022REVISED
2 May 2022PUBLISHED
19 May 2022

V Fantauzzo , S R Yeandel , C L Freeman and J H Harding

Department of Materials Science and Engineering, University of Sheffield, Sheffield, United Kingdom

E-mail: j.harding@sheffield.ac.uk**Keywords:** crystallisation, forcefield, simulation, nitratesSupplementary material for this article is available [online](#)

Original content from this work may be used under the terms of the [Creative Commons Attribution 4.0 licence](#).

Any further distribution of this work must maintain attribution to the author(s) and the title of the work, journal citation and DOI.

**Abstract**

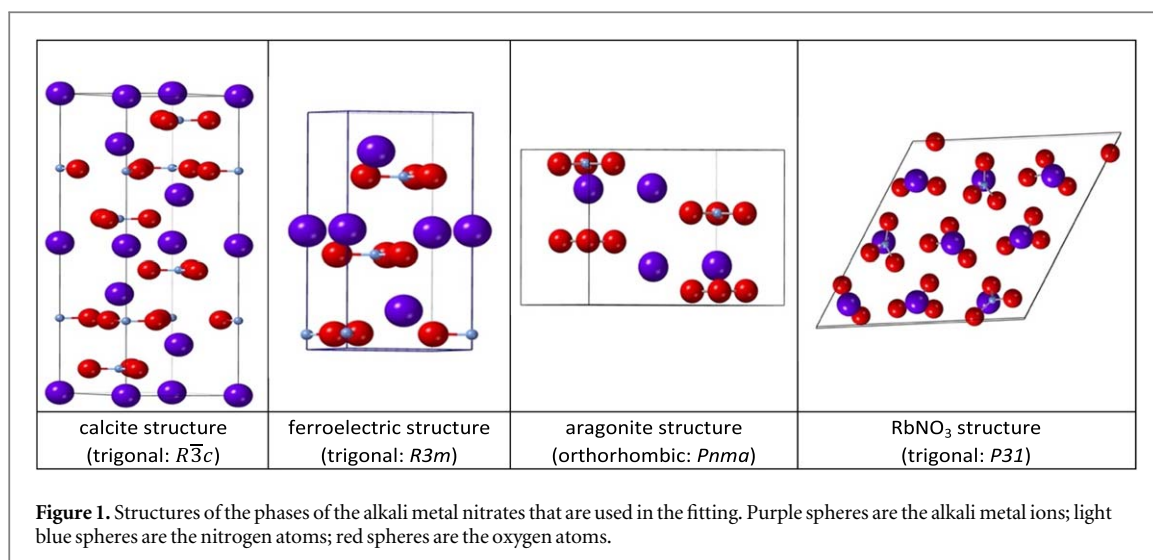
We present a new rigid-ion force-field for the alkali metal nitrates that is suitable for simulating solution chemistry, crystallisation and polymorphism. We show that it gives a good representation of the crystal structures, lattice energies, elastic and dielectric properties of these compounds over a wide range of temperatures. Since all the alkali metal nitrates are fitted together using a common model for the nitrate anion, the force-field is also suitable for simulating solid solutions. We use the popular Joung and Cheatham model for the interactions of the alkali metal cations with water and obtain the interaction of the nitrate ion with water by fitting to a hydrate.

1. Introduction

Nucleation and crystal growth are fascinating phenomena that require computationally expensive tools to be fully understood [1, 2]. Recent studies have focused on molecular anion systems, particularly carbonates, phosphates and sulphates, due to their biological and industrial relevance [3]. Alkali metal nitrates are made up of a monovalent cation and a simple triangular molecular ion. They show a widely diffused polymorphism which makes them interesting to study [4]. NaNO_3 has an extended second-order polymorphic transition and is a model for the isostructural calcite mineral (CaCO_3). KNO_3 is polymorphic: α - KNO_3 takes the aragonite structure; β - KNO_3 is trigonal; γ - KNO_3 is also trigonal but has no centre of symmetry; high pressure phases also exist. RbNO_3 has a rich polymorphism with four phases at ambient pressure. The stable polymorph (phase IV) at room temperature has a complex trigonal structure. The end members; LiNO_3 and CsNO_3 , are monomorphic. All alkali metal nitrates possess high solubility, so simulations are far better able to link to experimental conditions since smaller simulation boxes can be used.

Modelling these systems relies on good quality force-fields, which must be as accurate and consistent as possible without being computationally expensive. It is essential to balance computational cost against the ability of the simulation to reproduce the observed phenomena. A model must be transferable, so that it can be used for all the phases of a given nitrate and, if possible, the same representation of the nitrate anion should be used throughout so that solid solutions can be simulated (the nitrate ion is often kept rigid to simplify calculations, but we shall use a flexible model here). We focus on potassium nitrate because it presents polymorphs similar to those of calcium carbonate. The similarities between those two systems make potassium nitrate a good candidate for a model system to understand calcium carbonate itself. In this paper, we fit a reliable set of force-fields in order to be able to simulate the nucleation and growth of the alkali metal nitrates and use them to help understand the mechanisms of crystallisation.

Several previous force-fields have been developed (e.g. Hammond *et al* [5] (Li, Rb), Ribeiro *et al* [6] (Li, Na, K, Cs), Xie *et al* [7] (Li, Na, K), Ni *et al* [8] (Li, Na, K), Mort *et al* [9] (Na, K) and Jayaraman *et al* [10] (Li, Na, K)). These have been developed for high temperature molten mixtures (Ribeiro, Jayaraman), solutions (Hammond, Xie, Ni), and defect chemistry (Mort) but no force-field has been developed that can be used across all of the alkali metal nitrates and none of them are really suitable for investigating crystallisation. The shortcomings of the various existing force-fields are discussed in detail in the supplementary material (available online at stacks.iop.org/JPCO/6/055011/mmedia). Briefly, Ni, Xie and Mort fail to obtain the correct order for the relative energy



of polymorphs in some nitrates; Ribeiro fails to optimise several crystal structures; none of the models (except that of Hammond) predict real values for all the high-symmetry branches of the phonon spectra of the polymorphs to which they were fitted (showing that the true predicted structure must be of lower symmetry than the ones considered). The existing force-fields are adequate for the purposes they were intended for but there is clearly room for improvement. Also, there is no force-field that is suitable for all the alkali metal nitrates, their solution chemistry and their solid state solutions. Before we discuss details of the fitting, we review the structures of the alkali metal nitrates.

1.1. Structures of the alkali metal nitrates

1.1.1. Lithium nitrate

Crystallises in the rhombohedral $R\bar{3}c$ group at 290 K with $Z = 6$, $a = 4.692 \text{ \AA}$, $c = 15.2149 \text{ \AA}$ [11] (isostructural with calcite). So it will have a Bravais-Friedel-Donnay-Harker morphology showing $\{012\}$, $\{01\bar{2}\}$ and $\{001\}$ forms [12].

1.1.2. Sodium nitrate

Crystallises in the rhombohedral $R\bar{3}c$ group at 298 K with $Z = 6$, $a = 5.0396 \text{ \AA}$ and $c = 16.829 \text{ \AA}$ (II-NaNO₃) [13] and becomes a high-temperature disordered phase ($R\bar{3}m$; I-NaNO₃) at 548.5 K. This polymorph has $Z = 3$, $a = 5.0889 \text{ \AA}$ and $c = 8.868 \text{ \AA}$. The nitrate group appears to be static in the low temperature phase but undergoes rotational disorder in the high-temperature phase [14]. Both carbonate and nitrate groups show disordered high temperature phases. Starting from a pure solution it is possible to grow single $\{10.4\}$ rhombohedral crystals [15] whilst adding Li^+ and K^+ ions to the solution produces $\{00.1\}$ crystals [16].

1.1.3. Potassium nitrate

Exists in three different polymorphic forms at atmospheric pressure [17]: I, β -KNO₃ rhombohedral $R\bar{3}m$, stable at 403 K with $a = 5.42 \text{ \AA}$ and $c = 19.41 \text{ \AA}$ [18]; II, α -KNO₃ aragonite $Pnma$, stable at 299 K; $a = 6.2703 \text{ \AA}$, $b = 5.3935 \text{ \AA}$, $c = 9.1366 \text{ \AA}$ [19]; III γ -KNO₃, rhombohedral, $R\bar{3}m$, ferroelectric, stable at 397 K, with $a = 5.43 \text{ \AA}$ and $c = 9.112 \text{ \AA}$ [20]. On cooling phase III to 383 K it is possible to recover phase II. There is a metastable monoclinic phase (δ -KNO₃ [21]) and a high-pressure orthorhombic phase (IV) [22]. Below 305 K KNO₃ mostly has the growth forms $\{110\}$, $\{111\}$, $\{010\}$ and $\{021\}$ [4].

1.1.4. Rubidium and caesium nitrate

Crystallise in a complex trigonal structure ($Z = 9$; $P\bar{3}1$, $a = 10.55 \text{ \AA}$, $c = 7.47 \text{ \AA}$ (RbNO₃ at 298 K) [23] and $a = 10.902 \text{ \AA}$, $c = 7.74 \text{ \AA}$ (CsNO₃ at 296 K) [24].

Standard thermodynamic data is quoted in the literature for some of the polymorphs. Rao and Rao [25] discuss the enthalpies of transformation that are available. They conclude that the most reliable data are when there is agreement between the differential thermal analysis and calorimetric values. There are two examples known: for KNO₃ (phase II ($Pnma$) \rightarrow phase I ($R\bar{3}m$)); $\Delta H = 5.0 \text{ kJ mol}^{-1}$) and for RbNO₃ (phase IV ($P\bar{3}1$) \rightarrow phase III ($Pm\bar{3}m$)); $\Delta H = 4.0 \text{ kJ mol}^{-1}$). These small differences make reproducing the order of stability of the polymorphs a serious challenge. Figure 1 (below) shows the structures for the four space-groups where all the sites are fully occupied that have been used in the fitting process.

Table 1. Interactions between alkali metal ions [26] $q_M = 1.0$ for $M = \text{Li-Cs}$ where ε and R_{\min} are defined as the energy and interatomic distance at the minimum, i.e. we use the Lennard-Jones potential in the form

$$V(r) = \varepsilon \left[\left(\frac{R_{\min}}{r} \right)^{12} - 2 \left(\frac{R_{\min}}{r} \right)^6 \right].$$

Alkali ions	ε (eV)	R_{\min} (Å)
Li-Li	0.01459	1.582
Na-Na	0.01528	2.424
K-K	0.01860	3.186
Rb-Rb	0.01930	3.474
Cs-Cs	0.00390	4.042

Table 2. Force field parameters for the nitrate ion ($q_N = 0.7802|e|$, $q_O = -0.5934|e|$).

Interaction type	Force constants	Distances	Angles
$V_{NO}(r) = \frac{1}{2} k_2 (r - r_0)^2$	k_2 (eVÅ ⁻²) = 40.849	r_0 (Å) = 1.255	
$V_{NOO}(\theta) = \frac{1}{2} k_\theta (\theta - \theta_0)^2$	k_θ (eVrad ⁻²) = 13.234		θ_0 (deg) = 120.0
$V_{NOO}(r_{12}, r_{13}) = k_{bc}(r_{12} - r_{12}^0)(r_{13} - r_{13}^0)$	k_{bc} (eVÅ ⁻²) = 12.818	r_{12}^0 (Å) = 1.255 r_{13}^0 (Å) = 1.255	
$V_{NOO}(r_{12}, r_{13}, \theta) = [k_{bca}^{12}(r_{12} - r_{12}^0) + k_{bca}^{13}(r_{13} - r_{13}^0)](\theta - \theta_0)$	k_{bca}^{12} (eVÅ ⁻¹) = 1.533	k_{bca}^{13} (eVÅ ⁻¹) = 1.533	r_{12}^0 (Å) = 1.255 r_{13}^0 (Å) = 1.255 θ_0 (deg) = 120.0
$V_{NOOO}(d) = k_2^{oop} d^2 + k_4^{oop} d^4$	k_2^{oop} (eVÅ ⁻²) = 13.647	k_4^{oop} (eVÅ ⁻⁴) = 360.0	

2. Methodologies

We require a force-field that can describe alkali metal nitrates equally well in solution and as a solid phase. To keep the costs of molecular dynamics simulations down, a rigid ion model with flexible nitrate ions was used. This type of model has proved successful for many molecular ions, in particular the carbonates and sulphates. Full ionic charges ($q_M = 1$) are used for the alkali metal ions. The fitting of charges on the nitrogen and oxygen atoms is discussed below. Buckingham potentials were used for all intermolecular interactions except for those between the alkali metal cations where the Lennard-Jones form was used for consistency with the model of Joung and Cheatham [26], frequently used to study solution chemistry of the alkali halides. The parameters for these interactions are given in table 1.

A force-field developed by Raiteri *et al* [27] for the carbonate anion was used as a starting point for the nitrate but with the initial partial charges adjusted (using charges from electronic structure calculations as a guide) to give the correct overall charge on the nitrate anion and subsequently fitted to the crystal structures and properties as described below. To describe the interactions within the nitrate group, harmonic interactions were used for the N-O bond and three-body bond-angle potentials used to maintain the preferred angle between the bonds. Further many-body interactions were added (as specified by Raiteri *et al*) to maintain the planarity of the nitrate anion. Coulomb subtraction was applied within all the nitrate molecules. Examination of the Raman lines demonstrated that the internal interactions of the carbonate group could approximate the internal interactions of the nitrate group. The force-field for the nitrate anion is given in table 2. A tapering cut-off for the short-range intermolecular potentials was applied during the fitting. The basic interatomic interaction is multiplied by an additional mathematical function that smooths both its energy and derivatives to zero at the cut-off. The MDF [28] (Mei-Davenport-Fernando) taper was applied, which has the form

$$V_{smooth}(r) = V(r) \cdot f_{cut}(r) \quad (1)$$

where

$$f_{cut} = \begin{cases} 1 & r < r_m \\ (1 - x)^3(1 + 3x + 6x^2) & r_m \leq r < r_{cut} \\ 0 & r \geq r_{cut} \end{cases} \quad (2)$$

and $x = \frac{(r - r_m)}{(r_{cut} - r_m)}$. In this case, r_m was set at 6.0 Å and r_{cut} at 9.0 Å.

Table 3. Interactions between alkali metal ions and water [26] $q_M = 1.0$ for $M = \text{Li-Cs}$ where ε and R_{\min} are defined as the energy and interatomic distance at the minimum, i.e., the Lennard-Jones potential is written

$$\text{as } V(r) = \varepsilon \left[\left(\frac{R_{\min}}{r} \right)^{12} - 2 \left(\frac{R_{\min}}{r} \right)^6 \right].$$

Alkali ions	ε (eV)	R_{\min} (Å)
Li–O (H ₂ O)	0.009921	2.5676
Na–O (H ₂ O)	0.010152	2.9886
K–O (H ₂ O)	0.011207	3.3696
Rb–O (H ₂ O)	0.011406	3.5136
Cs–O (H ₂ O)	0.005125	3.7976
H ₂ O–H ₂ O	0.006740	3.553145

Table 4. SPE/Fw parameters for the water molecule ($q_H = 0.41|e|$, $q_O = -0.82|e|$) Wu *et al* [39] The water-water interaction is given in table 3.

Interaction type	Force constants		Distances		Angles	
$V_{HO}(r) = \frac{1}{2} k_2 (r - r_0)^2$	k_2 (eVÅ ⁻²)	45.93	r_0 (Å)	1.012		
$V_{HO}(\theta) = \frac{1}{2} k_\theta (\theta - \theta_0)^2$	k_θ (eVrad ⁻²)	3.291		θ_0 (deg)	113.24	

2.1. Fitting procedures

The GULP [29, 30] code was used to fit the force-fields using the relaxed fitting algorithm [31]. Details of the code, including the methods used to calculate the long-range electrostatic summations, can be found in [30]. An iterative procedure was used to obtain the charges on the nitrogen and oxygen atoms. First the individual nitrates were fitted to experimental data to obtain interactions between the alkali metal ions and the atoms of the nitrate anion. Then the nitrogen charge, q_N , and short-range oxygen-oxygen intermolecular interactions were refitted to data for the observed low temperature polymorphs of all the alkali earth nitrates together, assuming that the intramolecular interactions of the nitrate ions and the intermolecular interactions (including electrostatic interactions) between the nitrate ions were the same for all the alkali metal nitrates. The oxygen charge, q_O , is fixed by the requirement that the total charge of the nitrate anion be -1 . Then the alkali metal - nitrate interactions were re-fitted for each compound. This process was iterated until a self-consistent solution was obtained.

A considerable amount of experimental data is available for fitting the force-field. This includes structural data for many of the polymorphs, often at several temperatures (see the earlier discussion); elastic properties including the thermoelastic constants ($d[\log C_{ij}]/dT$) [32]; dielectric data [33] (more details are given in the supplementary information). Although partial occupancy can be modelled in GULP using a fractional occupation number, structures with partial occupancy were not used in the fitting process. Corrections need to be made to the available data before they can be compared with simulations. Lattice parameters obtained from experiment will be at a finite temperature and contain zero-point motion effects. Both these must be corrected for to compare with a lattice statics simulation (most often used in fitting). Lattice energies can be obtained from experiment and compared with the simulations, but individual enthalpies of formation are not easily usable since they require a model of the elements in their standard states.

We have performed density functional calculations using the CASTEP [34] (Cambridge Serial Total Energy Package) program to calculate the structures and properties of selected phases of the nitrates. This program uses a plane wave basis set to perform calculations on periodic systems. All the calculations were performed within the GGA approximation using the PBE functional [35] and adding dispersion corrections [36] (employing the DFT-D method [37]). Pseudopotentials were generated ‘on the fly’. The plane-wave energy cut-off was set at 800 eV; a Monkhorst-Pack grid was used for k-point sampling ($8 \times 8 \times 8$ grid, spacing 0.001 \AA^{-1}). Geometry optimisation was performed using the BFGS algorithm [38]. Since the force-field is needed for aqueous systems, we require a model for the interactions between water and the alkali earth cations and the nitrate anion. We use the SPC/Fw model for water [39] since it is cheap on computer resources and performs well in conjunction with the carbonate and sulphate anions. For completeness, the parameters for the interactions between alkali metal ions and water are listed in table 3 and those for the water model itself are listed in table 4.

Molecular dynamics simulations were performed to investigate the high-temperature behaviour of the force-fields. The DL_POLY [40] code was used to perform canonical ensemble calculations over a temperature

Table 5. Buckingham parameters fitted for a rigid ion force-field (unit charge for all metal ions).

Interaction	A (eV)	ρ (Å)	C (eVÅ ⁶)
Li–O	170.7	0.30063	0.0
Li–N	1155.8	0.260907	0.0
Na–O	1842.1	0.24778	0.0
Na–N	10598.7	0.2376	0.0
K–O	220.6	0.36777	0.0
K–N	4.99×10^{12}	0.09385	0.0
Rb–O	2324.9	0.28467	0.0
Rb–N	81681.5	0.20626	0.0
Cs–O	34792.7	0.22944	0.0
Cs–N	98642.0	0.22721	0.0
O–O	44806.0	0.20659	31.0

interval from 1 to 500 K to model lattice expansion. A Nosé-Hoover thermostat with a relaxation time of 0.1 ps was used. The time step was set to 0.5 fs. The selected number of time steps was 50000 (25 ps), of which 10000 (5 ps) were used as an equilibration period. A temperature-scaling interval of 10 K was used, whilst the radial distribution function (RDF) was collected every 1000 time steps, using a bin width of 0.1 Å to obtain the plot. The Ewald summation real space cut-off was set to 8.0 Å, whilst the width of the Verlet shell was 1 Å. The Ewald sum precision was set to a relative error of 10^{-5} . In order to calculate the long ranged electrostatic (coulombic) potentials the Smoothed Particle Mesh Ewald (SPME [41]) summation method was used. The grid for the k-vector summation was set with dimensions of $8 \times 8 \times 8$, and α , the Ewald splitting parameter, set to 0.36037 \AA^{-1} . Isothermal-isobaric (NPT) ensemble calculations were performed using the Nose-Hoover NPT ensemble, with the pressure set to 1 atm and the temperature changed from 300 K to 500 K. The thermostat and barostat relaxation times were 0.1 ps. Other parameters were set as for the NVT simulation.

2.2. Simulation of solution properties

To obtain the free energies of ion solvation we performed thermodynamic integration (TI) calculations with the LAMMPS code [42]. To perform a thermodynamic integration we must define a pathway between the two systems of interest, in this case the ion in solution and the ion in vacuum. The pathway must be continuous and reversible. The point along the pathway may be defined by the parameter λ . The free energy may then be obtained by integrating over this pathway.

$$\Delta A = \int_{\lambda=0}^{\lambda=1} \left\langle \frac{\partial U(\lambda)}{\partial(\lambda)} \right\rangle_{\lambda} d\lambda \quad (3)$$

where $U(\lambda)$ is the potential energy of the system at the point along the pathway given by λ . Hence the term in the angle brackets represents the average of the derivative of the potential energy with respect to λ over the course of a simulation at that λ value. We do not use λ directly but instead use a nonlinear function of λ

$$f(\lambda) = \lambda^5(70\lambda^4 - 315\lambda^3 + 540\lambda^2 - 420\lambda + 126) \quad (4)$$

The use of the nonlinear function stabilises the calculation of the system as λ approaches 0 or 1 [43]. Using the $f(\lambda)$ of (4) is equivalent to sampling more heavily near the tail end values of λ , with a reweighting scheme given by the derivative of $f(\lambda)$ with respect to λ . The derivative in equation (3) is obtained via the chain rule

$$\frac{\partial U(\lambda)}{\partial(\lambda)} = \frac{\partial U(f(\lambda))}{\partial f(\lambda)} \frac{\partial f(\lambda)}{\partial(\lambda)} \quad (5)$$

where the derivative of the nonlinear function with respect to λ is obtained analytically. The derivative of the potential energy with respect to the nonlinear function is obtained numerically by re-analysing the simulation trajectory and recalculating the potential energy with slightly perturbed values of $f(\lambda)$ and entering the result into a central differencing scheme for the computation of the derivative. The perturbed values of $f(\lambda)$ are chosen to be 1% of the value of $f(\lambda)$ to avoid unphysical negative force-field parameters arising in the central differencing scheme.

The pathway we choose between the solvated and desolvated ion is to deactivate all inter-molecular interactions between the ion and the water simultaneously. We construct a cubic simulation cell containing 3,200 water molecules and equilibrate in an NPT ensemble at 300 K and 0 atm pressure for 1 ns with lattice vectors averaged every 100 fs to get average lattice vectors for the correct density of pure water. We then insert a single ion into the simulation cell (either K or NO_3). This leads to a small additional pressure in the cell when the interactions of the water with the ion are at full strength but is negligible at the simulation cell sizes we use.

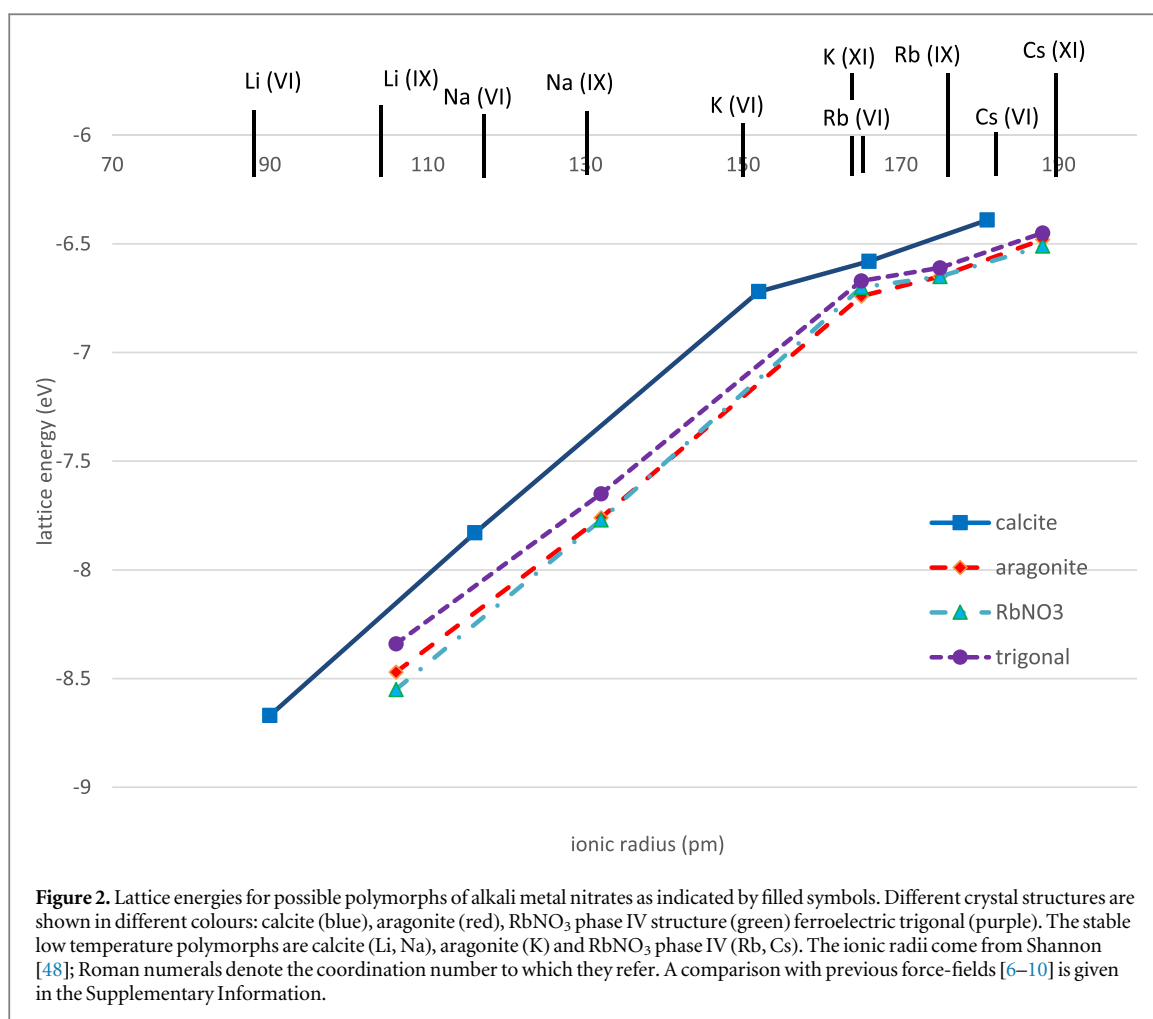


Table 6. Comparison between dielectric constants calculated using various force-fields and experimental values for the aragonite phase of potassium nitrate (KNO₃).

	ϵ_{11}	ϵ_{22}	ϵ_{33}
Expt [33]	2.28	1.56	2.25
Force-field (this work)	3.6	2.9	2.8
Force-field [6]	1.79	2.55	2.47
Force-field [7]	0.5	2.17	2.11
Force-field [8]	3.5	4.24	3.95
Force-field [9]	2.58	2.22	2.33
Force-field [10]	2.6	2.86	2.66

*Note that the axes have been changed from the original references to conform to the crystallographic axes used for the Pnma space group in [18].

The TI simulations were each run in an NVT ensemble for 1 ns with the trajectory printed for re-analysis every 100 fs. We ran 42 simulations at a λ interval of 0.025 (except below the point at 0.025 where the simulations became unstable, however this represents a small error in our calculation and may be excluded). The integration was performed using the trapezoidal rule to obtain the free energy of solvation.

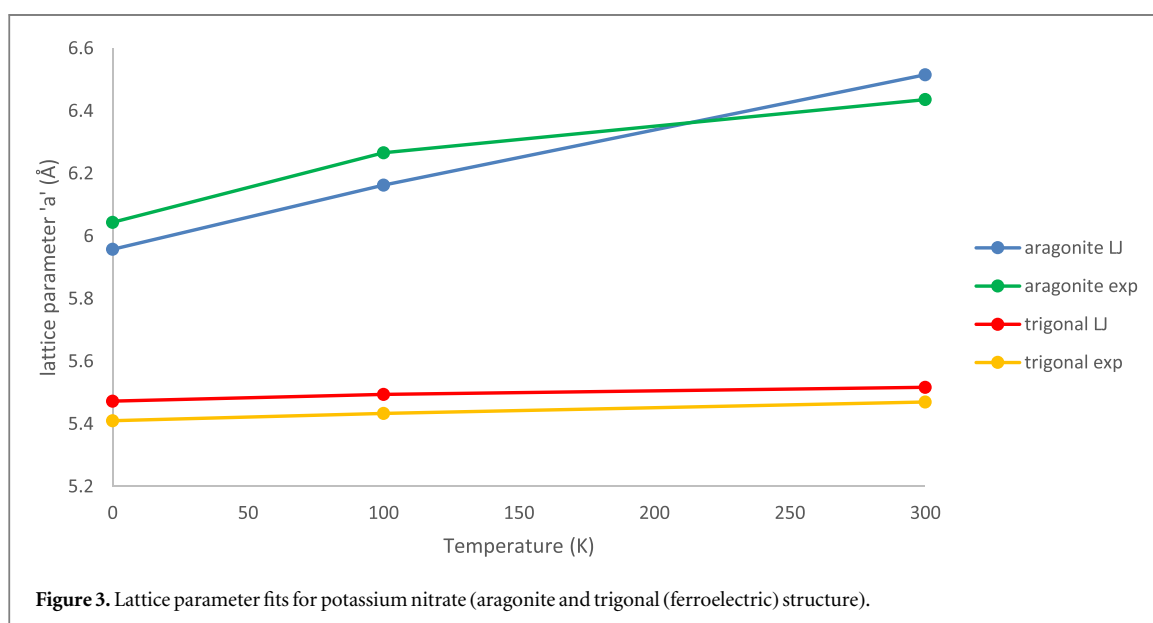
Comparison of our results with ‘experimental’ tabulations of free energies of solvation is not a simple matter. In addition to ensuring that the results are converged with respect to the size of the simulation cell, it is also necessary to correct for polarisation effects and for the electrostatic potential generated at the site of the ion in a manner consistent with the assumptions that underly the tabulations we wish to compare with. Such issues have been discussed by various authors [44–47] who have reached apparently different conclusions. We consider this matter in the next section.

Table 7. Comparison between elastic stiffness constants (GPa), calculated using various force-fields and density functional calculations and experimental values for the aragonite phase of potassium nitrate (KNO_3).

	C_{11}	C_{22}	C_{33}	C_{44}	C_{55}	C_{66}	C_{12}	C_{13}	C_{23}
Expt [32] ^{a,b}	26.1	49.7	40.7	10.5	9.6	7.0	12.8	14	22.1
Force-field (this work)	15.3	39.3	28.4	8.4	9.6	8.2	8.5	9.5	16.2
Force-field [6]	18.1	41.3	32.8	10.1	10.3	8.9	9.6	11	17.6
Force-field [7]	44.7	59.9	39.3	11.7	15.1	13.5	20.1	21.9	30.4
Force-field [8]	24.4	42.6	35.1	9.9	12.4	11.1	7.4	9	20
Force-field [9]	9.9	37.6	29.0	8.00	8.0	6.7	13.3	13.3	18.9
Force-field [10]	18.1	39.5	30.6	9.6	10.5	8.8	10.1	11.4	17.2
DFT (this work)	28.7	64.6	37.6	11.3	8.8	7.2	18.4	14.5	34.6
DFT [44]	21.9	40.2	32.9	9.6	8.8	7.3	10.4	12.1	17.3

^a Note that the axes (and hence the Voigt notation) for the elastic constants has been changed from the original references to conform to the crystallographic axes used for the Pnma space group in [18].

^b Values extrapolated back from the measured values at 293 K to 0 K using the thermo-elastic constants reported in the same paper [32].

**Figure 3.** Lattice parameter fits for potassium nitrate (aragonite and trigonal (ferroelectric) structure).

3. Results and discussion

We have fitted force-fields for all five alkali metal nitrates using the procedures outlined above. The parameters are given in table 5. Further details are given in the Supplementary Information but we summarise the main points here. We begin by investigating how well the various force-fields can describe the relative stability for all the polymorphs reported for alkali metal nitrates [4].

Figure 2 shows that the new force-field predicts (qualitatively) the correct stable polymorph for each of the alkali metal nitrates. It also predicts the correct structure for the only case where the crystal structure of a mixed alkali metal nitrate is known ($\text{NaRb}_2(\text{NO}_3)_3$). These results give confidence in the transferability of the forcefield. A fuller discussion of these issues, including the behaviour of other force-fields, is given in the Supplementary Information. We compared the predictions of the force-fields with experimental static dielectric constant data (table 6) and with elastic stiffness and crystal structure data obtained both from experiment and from *ab-initio* calculations (table 7). The lattice parameters are also in excellent agreement with experiment (the experimental lattice parameters are corrected to those for a static lattice i.e. the effects of temperature and zero-point vibrations are removed). The fit for the KNO_3 aragonite phase is shown in figure 3. Fits for the other alkali nitrates are in the Supplementary Information. Results for the density functional calculations of lattice parameters can also be found there.

The agreement with the experimental dielectric [33] and elastic constants (extrapolated to 0 K) [32] shown in tables 6 and 7 is as good as that obtained with previous sets of parameters where comparison is possible. Table 7 also shows that the forcefields compare reasonably well with the results of density functional calculations for the elastic properties. However, the new force-field improves on previous work in its ability to reproduce the

Table 8. Interactions between water and the nitrate anion using a Buckingham potential form $V(r) = A\exp(-r/\rho) - C/r^6$.

Interactions	A(eV)	ρ (Å)	C(eV Å ⁶)
H(H ₂ O)-O(NO ₃ ⁻)	577.7	0.226352	0.0
O(H ₂ O)-O(NO ₃ ⁻)	225677	0.18661	29.0

Table 9. Comparison with structural data for LiNO₃·3H₂O (space group Cmc₂m (63)) [45]. Comparison of the atomic positions can be found in Supplementary Information.

Lattice parameters	Expt	Force-field
<i>a</i> (Å)	6.8018	6.7756
<i>b</i> (Å)	12.7132	12.7464
<i>c</i> (Å)	5.9990	5.9296

experimental lattice dynamics. All previous force-fields show instabilities in the phonon spectra for at least some of the alkali nitrate polymorphs to which they were fitted except for those of Hammond [5]. This indicates that the structures obtained using previous force-fields were calculated using the full crystal symmetry and will distort away from the experimental crystal space group if the symmetry constraint is reduced or removed.

To obtain the interaction between the nitrate anion and the water molecules, we fit to the experimental crystal structure of the only known hydrate of the alkali metal nitrates, LiNO₃·3H₂O [45]. We assume the lithium interactions given in tables 1 and 5, the nitrate model of table 2 and the water model of table 4. We use mixing rules for the interactions between the nitrate oxygen and water oxygen atoms. This leaves only the interaction between the hydrogen atoms of water and the oxygen atoms of the nitrate ion to fit. All the parameters for the interactions between water and the nitrate ion are given in table 8 and the comparison with the structure of LiNO₃·3H₂O in table 9 with further details given in the Supplementary Information.

2.3. Simulation of free energies of hydration and solution structure

To demonstrate the reliability of the force field, we have calculated the free energy of hydration of the potassium and nitrate ions using the thermodynamic integration method described in the Methodology section. We must first consider the data which we are to use for the comparison. It is not possible to use experiments to measure the free energy of hydration of isolated ions; what can be measured is the thermodynamics of neutral combinations of ions. This can be used to infer the hydration free energies of isolated ions provided that the hydration free energy of one species can be fixed. The species chosen is usually the proton. So-called ‘conventional’ free energies are obtained by setting this quantity to zero. However, the free energies obtained by this route cannot be directly compared with simulations because of the arbitrary nature of this assumption. Hence a physically-based model must be used, usually based on the Born model of hydration. These issues are discussed in depth from the experimental perspective by Marcus [46, 47, 49], who is the author of the most extensive tables of thermodynamic parameters for the hydration of ions and more recently by Hofer and Hünenberger [50] from a theoretical perspective. Marcus [47] fixed the absolute free energy of a hydration for a proton at 298.15 K as -1056 ± 6 kJ mol⁻¹. It is now generally agreed from both theoretical [50] and experimental [51] research that a more accurate value is -1100 ± 14 kJ mol⁻¹. Marcus’ tabulated values must therefore be corrected by $-44z$ kJ mol⁻¹ where *z* is the charge of the ion. So his free energy of hydration for potassium (-295 kJ mol⁻¹) should be corrected to -339 kJ mol⁻¹ and his free energy of hydration for the nitrate ion (-300 kJ mol⁻¹) should be corrected to -256 kJ mol⁻¹.

Corrections must also be made to the simulation result. This is true whether spherical or periodic boundary conditions are used [52]. For periodic boundary conditions, the simulation of free energies of ion hydration uses a charged simulation cell, producing a divergence in the electrostatic summation which must be removed. The simplest way of doing this is to add a uniform neutralising correction to cancel the charge. This involves two types of correction. The first, (due to Fuchs [53]), corrects for the interaction of the charges with the neutralising background. The second (first discussed in [54], but usually called the Wigner correction) corrects for the self-energy of the added charge with its periodic images. Most codes using P³M (particle-particle-particle-mesh) approaches (such as LAMMPS, AMBER, DL_POLY) already include these terms, although this may not be immediately apparent (see [55] especially appendix A). Such codes do not include corrections for the artificial polarisation effects caused by the periodic boundary conditions. These are discussed in [56, 57]. Moreover, to connect with the absolute values for individual ions obtained by Marcus and others, we must ignore any effects

Table 10. Comparison between $r_{\max}(\text{N-O}_w)$ obtained in this work and available data in literature.

	$r_{\max}(\text{N-O}_w)$
Experimental [59]	$3.5 \pm 0.311 \text{ \AA}$
Xie et al [7]	3.65 \AA
Dang et al [60]	3.40 \AA
Banerjee et al [61]	3.50 \AA
This work	3.59 \AA

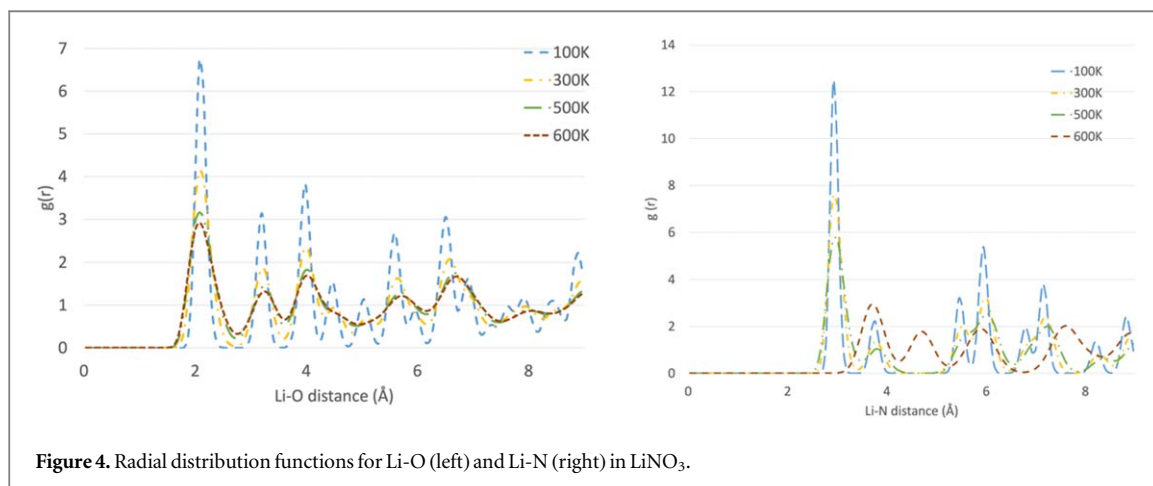


Figure 4. Radial distribution functions for Li-O (left) and Li-N (right) in LiNO_3 .

due to the transfer of the ion through the interface between the gas and water phases and subtract any effects due to the errors in the electrostatic potential at the site of the ion generated by the summation convention used for the electrostatics (see [51, 57, 58] for a full discussion and the importance of the distinction between ‘real’ and ‘intrinsic’ quantities when comparing with Marcus’ tables). There are also some small corrections arising from choice of thermodynamic conventions [47, 57]. Details are given in the Supplementary Information.

The raw thermodynamic integration results give -297 kJ mol^{-1} for the free energy of hydration of the potassium ion (the same as the value obtained by Joung and Cheatham [26] using the SPC/E model for water[#]). A hydration free energy of -311 kJ mol^{-1} was obtained for the nitrate ion. When the corrections are applied, these values become $-372.5 \text{ kJ mol}^{-1}$ (corrected Marcus value -339 kJ mol^{-1}) for the potassium ion and $-217.5 \text{ kJ mol}^{-1}$ (corrected Marcus value -256 kJ mol^{-1}) for the nitrate ion. However, it is important to remember that experimentally accessible quantities (such as the free energy of solution) depend only on the sum of the free energies of hydration of individual ions. Both the simulation corrections (arising from the electrostatic potential for the cation and anion) and the experimental corrections (arising from the choice of the free energy of hydration of the proton) cancel out. The simulated value for the sum of the free energies of cation and anion is -585 kJ mol^{-1} . The tabulated value obtained from Marcus is -595 kJ mol^{-1} - within about 2% showing excellent agreement.

Further tests using the force-field in water have been performed. Starting from a box of water and potassium nitrate, molecular dynamics simulations using DL_POLY in an NVT ensemble have been performed (2000 water molecules and 50 potassium nitrate formula units). The radial distribution function (RDF) for KNO_3 -water was extracted and analysed (see figure 3). The first maximum in the RDF for the nitrogen in the nitrate ion and the oxygen in the water molecule ($r_{\max}(\text{N-O}_w)$) is at 3.59 \AA , which shows good agreement with those found in literature, as can be seen from table 10.

The number of water oxygen atoms around the nitrate nitrogen has also been calculated, by integrating the RDF. The coordination number obtained (9.6) shows a good agreement with the values from previous literature as it is possible to see in table 11.

2.4. Simulation of the crystal structures at high temperature

We finally turn to a more detailed consideration of the structures predicted by the simulations. NPT molecular dynamics simulations were performed as previously described and showed that for the lithium nitrate system the structure is calcite-like (space group $R\bar{3}c$) at all temperatures and peaks retain their shape (figure 4). The structure loses some long-range order when the system is heated up from 100 K to 500 K (peaks between 4.5 and 5 \AA and between 5 and 7.8 \AA merge). However, changes in the polymorph are not visible (lithium nitrate is

Table 11. Comparison between coordination number obtained in this work and available data in literature.

	Coordination number
Xie <i>et al</i> [7]	10 ± 1
Dang <i>et al</i> [60]	12
Banerjee <i>et al</i> [61]	9.2
This work	9.6

[#]The most important correction omitted by Joung and Cheatham is the one involving the electrostatic potential at the site of the cation. When this is added, their result for the free energy of hydration of the potassium ion becomes -371 kJ mol^{-1} .

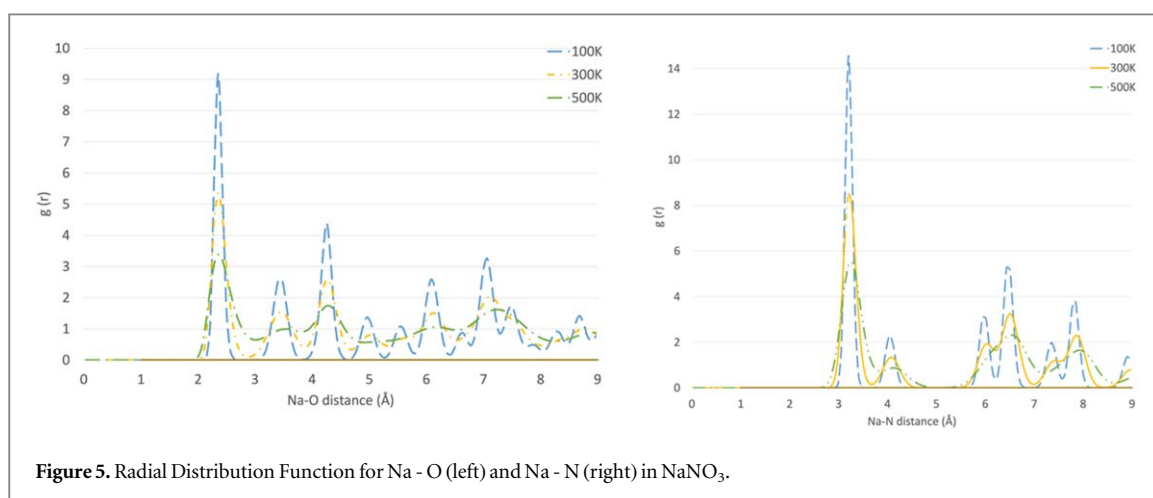


Figure 5. Radial Distribution Function for Na - O (left) and Na - N (right) in NaNO_3 .

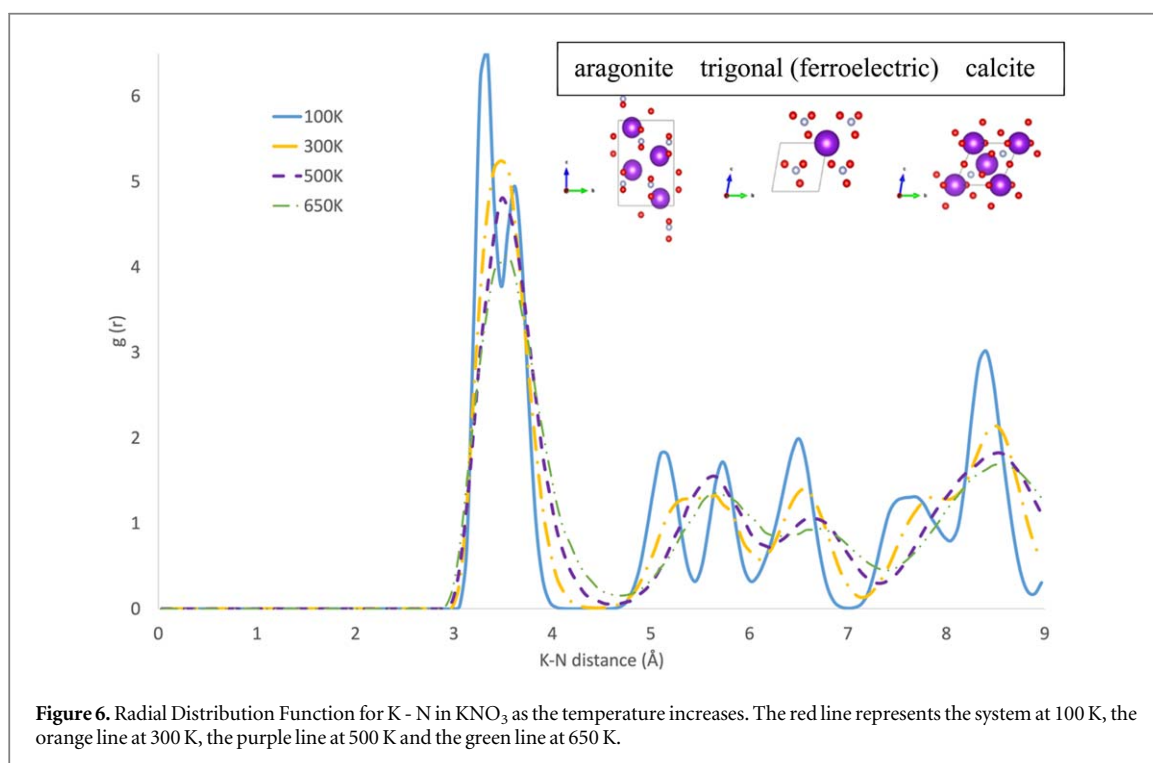
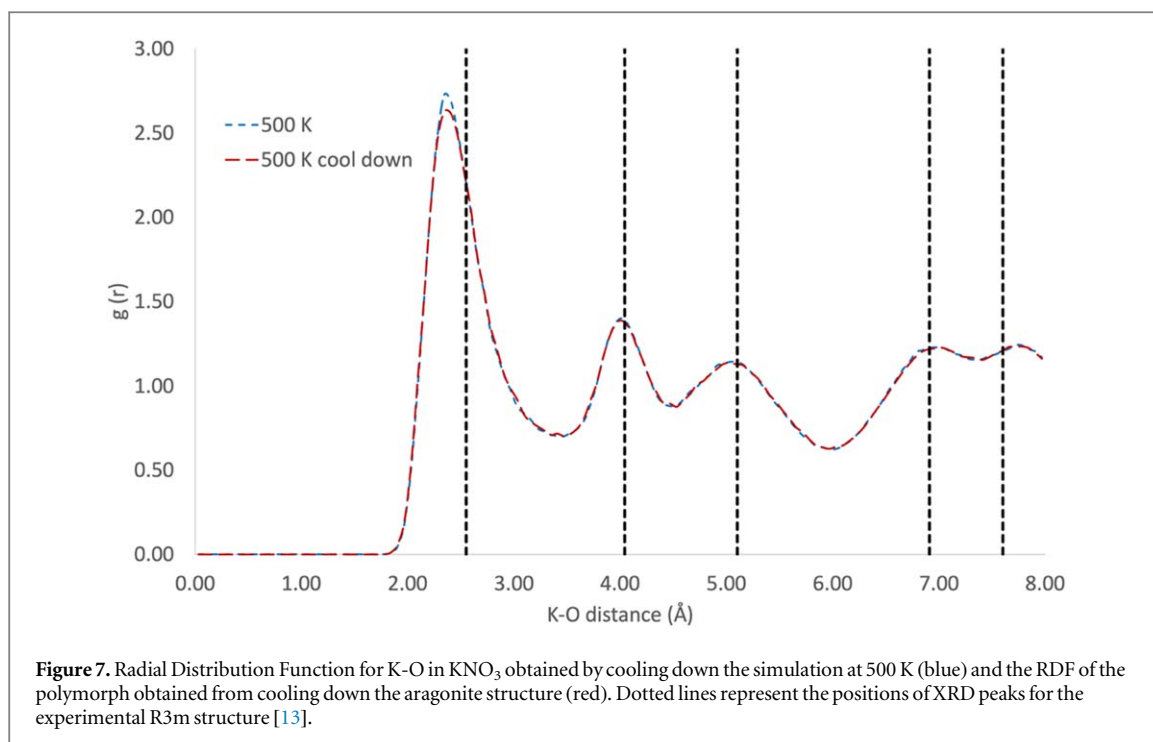


Figure 6. Radial Distribution Function for K - N in KNO_3 as the temperature increases. The red line represents the system at 100 K, the orange line at 300 K, the purple line at 500 K and the green line at 650 K.

monotropic as experimentally reported). If the temperature is raised to 600 K the long-range order decays further (peaks shift to the right/broaden and their height decreases). At greater atomic separations, the lack of coherence becomes more evident with more peaks merging (around 6, 7 and 9 Å). The behaviour is similar for



sodium nitrate (figure 5). At all temperatures the structure is calcite-like (space group $R\bar{3}c$); the peaks lose their shape as the temperature rises.

Potassium nitrate is a more interesting case to study, because the RDFs show evidence for three different polymorphs (see figure 6): the ferro-electric trigonal structure (space group $R3m$) at 100 K; the aragonite structure at 300 K and the trigonal $R\bar{3}m$ structure, (quasi-calcite form) at 500 K. On cooling down the system returns to the original structure but not directly. Cooling down the 500 K trigonal structure gives a distorted aragonite structure, whereas the 300 K structure returns to the ferro-electric trigonal form on further cooling. This suggests that the force field is able to reproduce the polymorph changes and shows that those changes are temperature-dependent (potassium nitrate is enantiotropic). Figure 7 shows the good agreement between the experimental K-O distances obtained by X-ray diffraction and those obtained by simulation.

3. Conclusions

In this paper we discussed the need for a reliable, transferable force field for the alkali metal nitrates that can be used for all the nitrates including solid solutions. Our force-field reproduces the order of stability of the polymorphs for each alkali nitrate, the crystal structures of the polymorphs together with the elastic and dielectric properties of the materials where these are available. Stable phonon spectra (i.e. no imaginary modes) are obtained in all cases. The model also behaves well as a function of temperature, reproducing the experimental lattice expansion and also showing the transformation of the structures to disordered forms (due to the thermally activated rotation of the nitrate groups) where appropriate. The model is also compatible with the well-known model of Joung and Cheatham [26] for alkali metal ions in solution. Future work will demonstrate the application of this model to aqueous interfaces and crystallisation.

Acknowledgments

We acknowledge the Engineering and Physical Sciences Research Council (EPSRC) for funding via Programme Grant No. EP/R018820/1 which funds the ‘Crystallisation in the Real World’ Consortium. Via our membership of the UK’s HEC Materials Chemistry Consortium, which is funded by EPSRC (EP/R029431), this work used the ARCHER2 UK National Supercomputing Service (<http://www.archer2.ac.uk>). VF thanks EPSRC for the provision of a studentship. For the purpose of open access, the author has applied a Creative Commons Attribution (CC BY) licence to any Author Accepted Manuscript version arising

Data availability statement

All data that support the findings of this study are included within the article (and any supplementary files).

Associated content

Supplementary information: Calculating the corrections to the free energy of hydration, comparison of force-fields with crystal structures, stability of polymorphs, comparison with crystal properties, the lattice thermal expansion and RDF functions (PDF)

Conflict of interest statement

The authors declare that there are no conflicts of interest.

ORCID iDs

V Fantauzzo  <https://orcid.org/0000-0001-7464-8772>

S R Yeandel  <https://orcid.org/0000-0002-6977-1677>

C L Freeman  <https://orcid.org/0000-0002-6326-1211>

J H Harding  <https://orcid.org/0000-0001-8429-3151>

References

- [1] Sosso G C, Chen J, Cox S J, Fitzner M, Pedevilla P, Zon A and Michaelides A 2016 Crystal nucleation in liquids, open questions and future challenges in molecular dynamics simulations *Chem. Rev.* **116** 7078
- [2] Jehannin M, Rao A and Cölfen H 2018 New horizons of non-classical crystallisation *J. Amer. Chem. Soc.* **141** 10120
- [3] Berce J, Zupančič M, Može M and Golobič I 2021 A review of crystallisation fouling in heat exchangers *Processes* **9** 1356
- [4] Benages-Vilau R, Calvet T and Cuevas-Diarte M À 2014 Polymorphism, crystal growth, crystal morphology and solid-state miscibility of alkali nitrates *Cryst. Rev.* **20** 25
- [5] Hammond R B, Orley M J, Roberts K J, Jackson R A and Quayle M J 2009 An examination of the influence of divalent cationic dopants on the bulk and surface properties of $\text{Ba}(\text{NO}_3)_2$ associated with crystallization *Cryst. Growth Des.* **9** 2588
- [6] Ribeiro M C C 2002 On the Chemla effect in molten alkali nitrates *J. Chem. Phys.* **117** 266
- [7] Xie W J, Zhang Z and Gao Y Q 2016 Ion pairing in alkali nitrate electrolyte solutions *J. Phys. Chem. B* **120** 2343
- [8] Ni H, Wu J, Sun Z, Lu G and Yu J 2019 Molecular simulation of the structure and physical properties of alkali nitrate salts for thermal energy storage *Renew. Energy* **136** 955
- [9] Mort K A, Wilde P J and Jackson R A 1999 Computer modelling of ammonium nitrate: I. Development of potentials and calculation of lattice properties *J. Phys. Condens. Matter* **11** 3967
- [10] Jayaraman S, Thompson A P, von Lilienfeld O A and Maginn E J 2010 Molecular simulation of the thermal and transport properties of three alkali nitrate salts *Ind. Eng. Chem. Res.* **49** 559
- [11] Wu X, Fronczek F and Butler L 1994 Structure of LiNO_3 —point-charge model and sign of the Li—7 quadrupole coupling-constant *Inorg. Chem.* **33** 1363
- [12] Aquilano D, Benages-Vilau R, Bruno M, Rubbo M and Massaro F R 2013 Positive and negative form of calcite crystal (CaCO_3) in the light of bravais-friedel-donnay-harker and hartman-perdok approach *Cryst. Eng. Comm.* **15** 4465
- [13] Gonschorek G, Weitzel H, Miede G and Schmahl W 2000 The crystal structure of NaNO_3 at 100 K, 120 K, and 563 K *Z. Krist.* **215** 752
- [14] Harris M J 1999 A new explanation for the unusual critical behaviour of calcite and sodium nitrate, NaNO_3 *Am. Min.* **84** 1632
- [15] Benages-Vilau R, Rubbo M, Calvet T, Aquilano D and Cuevas-Diarte M À 2013 Growth Kinetics of the {10.4} faces of nitratine (NaNO_3) *Cryst. Growth Des.* **13** 3419
- [16] Benages-Vilau R, Calvet T, Pastero L, Aquilano D and Cuevas-Diarte M À 2015 Morphology change of nitratine (NaNO_3) from aqueous solution, in the presence of Li^+ and K^+ Ions *Cryst. Growth Des.* **15** 5338
- [17] Rao C N R, Prakash B and Natarajan M 1975 *Crystal Structure Transformations In Inorganic Nitrites, Nitrates, and Carbonates* (Washington: National Standard Reference Data System-National Bureau of Standards)
- [18] Fugel M, Kleemiss F, Malaspina L A, Pal R, Spackman P R, Jayatilaka D and Grabowsky G 2018 Investigating the resonance in nitric acid and the nitrate anion based on a modern bonding analysis *Aust. J. Chem.* **71** 227
- [19] Nimmo J K and Lucas B W 1976 The crystal structures of gamma- and beta- KNO_3 and the alpha-gamma-beta transformations *Acta Cryst. B* **32** 1968
- [20] Freney E F, Garvie L A J, Groy T L and Buseck P R 2009 Growth and single-crystal refinement of phase-III potassium nitrate, KNO_3 *Acta Cryst. B* **65** 659
- [21] Wolf S, Alam N and Feldmann C 2015 Delta- KNO_3 : synthesis and structure of a new modification of potassium nitrate *Z. für Anorg. und Allg. Chem.* **641** 383
- [22] Worlton T G, Decker D L, Jorgensen J D and Kleb R 1986 Structure of high-pressure KNO_3 - IV *Physica B + C* **136** 503
- [23] Shamsuzzoha M and Lucas B W 1982 Structure (neutron) of phase IV rubidium nitrate at 298 and 403 K *Acta Cryst.* **38** 2353
- [24] Pohl D and Gross T 1993 Cesium nitrate (II) at 296 K *Acta Cryst.* **C 49** 316
- [25] Rao K J and Rao C N R 1966 Crystal structure transformations of alkali sulphates, nitrates and related substances: thermal hysteresis in reversible transformations *J. Mater. Sci.* **1** 238
- [26] Joung S and Cheatham T E 2008 Determination of Alkali and halide monovalent ion parameters for use in explicitly, solvated biomolecular simulations *J. Phys. Chem. B* **112** 9020

- [27] Raiteri P, Gale J D, Quigley D and Rodger P M 2010 Thermodynamically consistent force field for molecular dynamics simulations of alkaline-earth carbonates and their aqueous speciation *J. Phys. Chem. C* **114** 5997
- [28] Mei J, Davenport J W and Fernando G W 1991 Analytic embedded-atom potentials for fcc metals: application to liquid and solid copper *Phys. Rev. B* **43** 4653
- [29] Gale J D 1997 GULP: a computer program for the symmetry-adapted simulation of solids *J. Chem. Soc. Faraday Trans.* **93** 629
2005 *GULP: Capabilities and prospects Z. Kristall.* **200** 552–554
- [30] Gale J D GULP version 5.2: General Utility Lattice Program (accessed 10th Feb 2022) <https://gulp.curtin.edu.au/gulp>.
- [31] Gale J D 1996 Empirical potential derivation for ionic materials *Philos. Mag. B* **73** 3
- [32] Haussühl S 1990 Elastic properties of the nitrates of lithium, sodium, potassium, cesium, silver and thallium *Z. für Kristall.* **190** 111
- [33] Mansingh A and Smith A M 1971 Dielectric and conductivity studies in potassium nitrite and potassium nitrate *J. Phys. D: Appl. Phys.* **4** 560
- [34] Clark S J, Segall M D, Pickard C J, Hasnip P J, Probert M J, Refson K and Payne M C 2005 First principles methods using CASTEP *Z. Kristall.* **220** 567
- [35] Burke K 2012 Perspective on density functional theory *J. Chem. Phys.* **136** 150901
- [36] London F 1930 Zur Theorie und Systematik der Molekularkräfte *Z. für Phys.* **63** 245
- [37] Grimme S, Antony J, Ehrlich S and Krieg H 2010 A consistent and accurate *ab initio* parametrization of density functional dispersion correction (DFT-D) for the 94 elements H-Pu *J. Chem. Phys.* **132** 154104
- [38] Perdew J P, Burke K and Ernzerhof M 1996 Generalized Gradient Approximation Made Simple *Phys. Rev. Lett.* **77** 3865
- [39] Wu Y, Tepper H L and Voth G A 2006 Flexible simple point-charge water model with improved liquid-state properties *J. Chem. Phys.* **124** 024503
- [40] Smith W and Forester T R 1996 DL_POLY_2.0: a general-purpose parallel molecular dynamics simulation package *J. Molec. Graphics* **14** 136
- [41] Essmann U, Perera L, Berkowitz M L, Darden T, Lee H and Pedersen L G 1995 A smooth particle mesh ewald method *J. Chem. Phys.* **103** 8577
- [42] Plimpton S 1995 Fast parallel algorithms for short-range molecular dynamics *J. Comp. Phys.* **117** 1
- [43] de Koning M and Antonelli A 1996 Einstein crystal as a reference system in free energy estimation using adiabatic switching *Phys. Rev. E* **53** 465
- [44] Korabel'nikov D V and Zhuraviev Y N 2017 First-principles study of the elastic properties of nitrates *Russ. Phys. J.* **59** 2122
- [45] Hermansson K, Thomas J O and Olovsson I 1980 Hydrogen bond studies. CXXXVIII. Neutron diffraction studies of $\text{LiNO}_3(\text{H}_2\text{O})_3$ at 120 and 295 K *Acta Cryst B* **36** 1032
- [46] Marcus Y 1986 The hydration entropies of ions and their effects on the structure of water *J. Chem. Soc. (Farad. Trans. 1)* **82** 233
- [47] Marcus Y 1987 The thermodynamics of solvation of ions Part 2. - the enthalpy of hydration at 298.15 K *J. Chem. Soc. (Farad. Trans. 1)* **83** 339
- [48] Shannon R D 1976 Revised effective ionic radii and systematic studies of interatomic distances in halides and chalcogenides *Acta Cryst. A* **32** 751
- [49] Marcus Y 1991 Thermodynamics of solvation of ions. Part 5.—gibbs free energy of hydration at 298.15 K *J. Chem. Soc. (Farad Trans)* **87** 2995
- [50] Hofer T S and Hünenberger P H 2018 Absolute proton hydration free energies, surface potential of water, and redox potential of the hydrogen electrode from first principles: QM/MM free-energy simulations of sodium and potassium hydration *J. Chem. Phys.* **148** 222814
- [51] Malloum A, Fifen J J and Conradie J 2021 Determination of the absolute solvation free energy and enthalpy of the proton in solutions *J. Mol. Liq.* **322** 114919
- [52] Darden T, Pearlman D and Pedersen L G 1998 Ionic charging free energies: Spherical versus periodic boundary conditions *J. Chem. Phys.* **109** 10921
- [53] Fuchs K 1935 A quantum mechanical investigation of the cohesive forces of metallic copper *Proc. Roy. Soc. A* **151** 585–602
- [54] Leslie M and Gillan M J 1985 The energy and elastic dipole tensor of defects in ionic crystals calculated by the supercell method *J. Phys. C* **18** 973
- [55] Ballenegger V, Cerda J J, Lenz O and Holm C 2008 The optimal P^3M algorithm for computing electrostatic energies in periodic systems *J. Chem. Phys.* **128** 034109
- [56] Hummer G, Pratt L R and Garcia A E 1996 Free energy of ionic hydration *J. Chem. Phys.* **100** 1206
- [57] Hummer G, Pratt L R and Garcia A E 1997 Ion sizes and finite-size corrections for ionic solvation free energies *J. Chem. Phys.* **107** 1275
- [57] Kastenholz M A and Hünenberger P H 2006 Computation of methodology-independent ionic solvation free energies from molecular simulations. I. The electrostatic potential in molecular liquids *J. Chem. Phys.* **124** 124106
- [57] Kastenholz M A and Hünenberger P H 2006 II The hydration free energy of the sodium cation *J. Chem. Phys.* **124** 224501
- [58] Simonson T, Hummer G and Roux B 2017 Equivalence of M- and P-summation in calculations of ionic free energies *J. Phys. Chem. A* **121** 1525
- [59] Caminiti R, Licheri G, Piccaluga G and Pinna G 1978 *J. Chem. Phys.* **68** 1967
- [60] Dang L X, Chang T M, Roeselova M, Garrett B M and Tobias D J 2006 *J. Chem. Phys.* **124** 066101
- [61] Banerjee P, Yashonath S and Bagchi B 2016 Coupled jump rotational dynamics in aqueous nitrate solutions *J. Chem. Phys.* **145** 234502